ACS OMEGA

http://pubs.acs.org/journal/acsodf

Article

Synthesis and Antitrypanosomal and Mechanistic Studies of a Series of 2-Arylquinazolin-4-hydrazines: A Hydrazine Moiety as a Selective, Safe, and Specific Pharmacophore to Design Antitrypanosomal Agents Targeting NO Release

Angel H. Romero,* Elena Aguilera, Lourdes Gotopo, Jaime Charris, Noris Rodríguez, Henry Oviedo, Belén Dávila, Gustavo Cabrera, and Hugo Cerecetto*

Cite This: *ACS Omega* 2022, 7, 47225−47238

Read Online

ACCESS | Metrics & More | Article Recommendations | Supporting Information

ABSTRACT: Nitric oxide (NO) represents a valuable target to design antitrypanosomal agents by its high toxicity against trypanosomatids and minimal side effects on host macrophages. The progress of NO-donors as antitrypanosomal has been restricted by the high toxicity of their agents, which usually is based on NO-heterocycles and metallic NO-complexes. Herein, we carried out the design of a new class of NO-donors based on the susceptibility of the hydrazine moiety connected to an electron-deficient ring to be reduced to the amine moiety with release of NO. Then, a series of novel 2-arylquinazolin-4-hydrazine, with the potential ability to disrupt the parasite folate metabolism, were synthesized. Their in vitro evaluation against *Leishmania* and *Trypanosoma cruzi* parasites and mechanistic aspects were investigated. The compounds displayed significant leishmanicidal activity, identifying three potential candidates, that is, **3b**, **3c**, and **3f**, for further assays by their good antiamastigote activities against *Leishmania braziliensis*, low toxicity, non-mutagenicity, and good ADME profile. Against *T. cruzi* parasites, derivatives **3b**, **3c**, and **3e** displayed interesting levels of activities and selectivities. Mechanistic studies revealed that the 2-arylquinazolin-4-hydrazines act as either antifolate or NO-donor agents. NMR, fluorescence, and theoretical studies supported the fact that the quinazolin-hydrazine decomposed easily in an oxidative environment via cleavage of the N−N bond to release the corresponding heterocyclic-amine and NO. Generation of NO from axenic parasites was confirmed by the Griess test. All the evidence showed the potential of hydrazine connected to the electron-deficient ring to design effective and safe NO-donors against trypanosomatids.

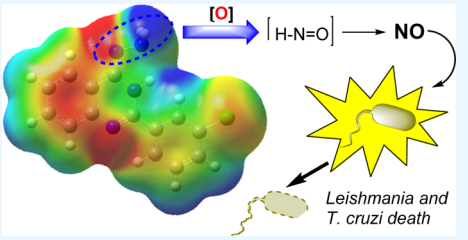

INTRODUCTION

Neglected tropical diseases (NTDs) such as leishmaniasis and Chagas disease are caused by obligate intracellular parasites of *Leishmania* spp. and *Trypanosoma cruzi*, respectively, which are transmitted to humans by insects.[1] Chagas disease is located in 21 countries of Latin America with approximately 6−7 million infected and more than 70 million people at risk,[2] whereas the leishmaniasis is prevalent in 88 countries worldwide with 350 million people at risk of acquiring the disease.[3]

At the moment, treatments against these NTDs are severely limited and only a few approved drugs are present: (i) benznidazol and nifurtimox against Chagas disease and (ii) pentavalent antimonials (e.g., glucantime and pentostam) against Leishmaniasis. A second line of anti-Chagas drugs such as antifungal azoles (e.g., osaconazole, ketoconazole, ravuconazole, etc.) and leishmanicidal agents including pentamidine, amphotericin B, and miltefosine are frequently used when the first line failed.[4] However, these drugs present several disadvantages including high toxicity (affecting the heart, liver, and kidneys), mutagenicity, high costs, low efficiency, and complex administration protocols.[4] As a consequence of the emergent parasite resistance, toxicity issues, and the lack of efficacy of these types of clinical agents against NTDs, new effective and safer drugs are urgently needed to open new lights toward the solution of these public health problems. Designing a specific and selective anti-trypanosomal agent is essential to know about the pivotal aspect in the survival of parasites. It is well documented that NO is a molecule considerably toxic for trypanosomatids and its production, for example, by infected macrophages as an immunological response, affects the cell proliferation of *T. cruzi* and *Leishmania* parasites into mammal cells.[5−7] Then, the in situ release of NO via drug decomposition or via immunologic activation represents an attractive strategy to design selective antitrypanosomal agents. Nowadays, there are a few examples

Received: October 6, 2022
Accepted: November 23, 2022
Published: December 6, 2022

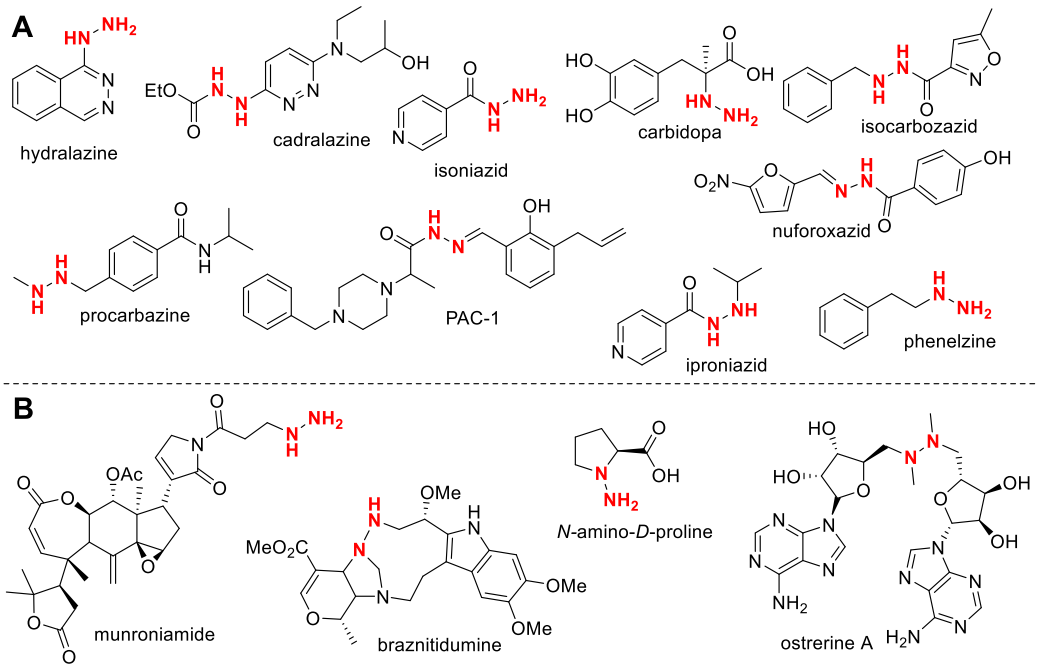

Figure 1. Hydrazines/hydrazides containing therapeutic agents (A) and natural products (B).

Chart 1. Principle Design of 2-Arylquinazolin-4-hydrazines Targeting Dual Action: (i) NO-Donor and (ii) Folate Inhibitor.

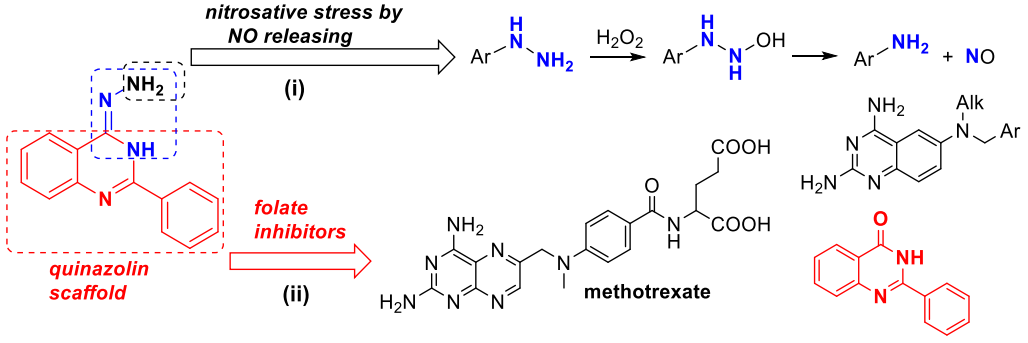

of antitrypanosomal agents targeting NO production.[7] Most of them are represented by metallic complexes containing the NO-ligand, which release NO through cleavage from the metal−NO bond.[8−12] Other examples consisted of organic NO-donor heterocycles, which are able to release NO via ring opening of the hetero-ring-masked NO-releasing moiety.[13−15] Despite good antitrypanosomal activity of compounds based on two mentioned chemical systems, the low selectivity with toxicity consequences is the main limitation of the NO-donors, in which the design of the new chemical form to access the NO in situ without side effects on host cells is important.

In this sense, the hydrazine (−NH_2−NH_2−) function represents an attractive moiety to design NO-donors because of the fact that the chemical functionality has shown to be highly sensitive to decompose via the oxidative process under basic or neutral conditions with generation of NO. For example, Rehse and Shahrouri showed the ability of a hydrazine moiety connected to an electron-deficient aromatic ring (e.g., phthalazine) to induce the release of NO in solution upon oxidative conditions, which was attributed to a plausible oxidative decomposition of the hydrazine moiety.[16] Other examples have shown the susceptibility of the hydrazine moiety to decompose in the presence of catalytic transition metals at room temperature.[17−19] Nevertheless, the use of hydrazine as a pharmacophore represents a controversial topic within medicinal chemistry because it is considered a promiscuous group.[20] In our favor, we can mention that there are a large number of approved drugs containing the hydrazine moiety with clinical uses including hydralazine and cadralazine as antihypertensives, isoniazid, isocarboxazid, and nifuroxazid as antibiotics, procarbazine as antineoplastic, phenelzine and iproniazid as antidepressants, and carbidopa as the anti-Parkinson drug (Figure 1A).[21,22] Also, the hydrazine can be found in natural products with biological activity.[23,24] Sperry and Blair showed that over 200 natural products contain the N−N bond motif, although only four of them presented the simple hydrazine moiety, including *N*-amino-*D*-proline, munroniamide, braznitidumine, and ostarine A (Figure 1B). Recently, the incorporation of the hydrazine moiety has received great attention for the development of active compounds against diverse types of pathologies.[25−29] Regarding the use of hydrazine to design leishmanicidal agents, aminoquinoline derivatives hybridized with the isoniazid or hydrazine group have promoted a good leishmanicidal activity against intracellular amastigotes of *Leishmania braziliensis* without an apparent cytotoxic effect.[15,30,31]

https://doi.org/10.1021/acsomega.2c06455
ACS Omega 2022, 7, 47225−47238

Scheme 1. Synthesis of 2-Aryl-quinazolin-4-hydrazine 3a−k[a]

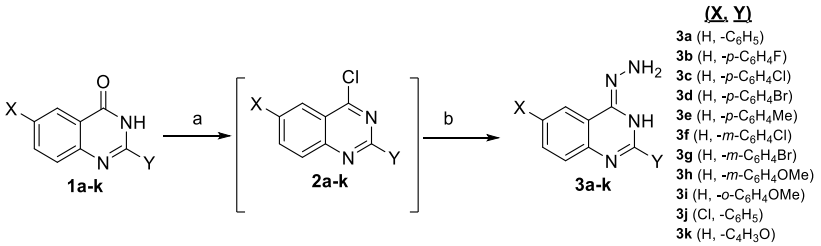

[a]Conditions: (a) 2-arylquinazolin-4(3*H*)-ones **1a−k**, $POCl_3$ (6 equiv), 100 °C, 4−5 h and (b) compound **2a−k**, $NH_2-NH_2{\cdot}xH_2O$ (4 equiv), ethanol, 70 °C, 2 h.

Table 1. In Vitro Growth Inhibitory Effects of the Compounds 3a−k and 4a−c and References Against *Leishmania* and *T. cruzi*

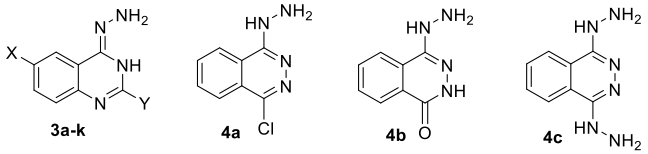

		promastigote, IC_{50} (μM) (PGI)[a]		epimastigote, IC_{50} (μM) (PGI)[a]
	compounds	*L. braziliensis*	*L. infantum*	*T. cruzi*
1	**3a**	**4.53 ± 0.23**	12.67 ± 0.74	>25.00 (42.7)
2	**3b**	**3.85 ± 0.17**	**5.01 ± 0.31**	17.95 ± **1.21**
3	**3c**	**5.12 ± 0.32**	**1.56 ± 0.09**	**11.48 ± 0.49**
4	**3d**	**6.20 ± 0.38**	**2.13 ± 0.12**	**14.32 ± 0.87**
5	**3e**	**10.06 ± 0.48**	**1.20 ± 0.08**	**17.99 ± 1.11**
6	**3f**	**5.63 ± 0.36**	**4.55 ± 0.29**	>25.00 (38.0)
7	**3g**	>25.0 (27.3)[a]	21.14 ± 1.21	>25.00 (21.4)
8	**3h**	12.21 ± 0.76	>25.0 (47.2)	>25.00 (10.1)
9	**3i**	>25.0 (49.23)[a]	>25.0 (28.3)	>25.00 (11.9)
10	**3j**	>25.0 (43.23)[a]	19.67 ± 1.78	>25.00 (37.7)
11	**3k**	>25.0 (46.56)[a]	14.03 ± 0.91	>25.00 (8.56)
12	**4a**	>25.0 (20.12)[a]	>25.0 (18.56)	>25.0 (10.22)
13	**4b**	>25.0 (18.56)[a]	>25.0 (12.34)	>25.0 (9.66)
14	**4c**	>25.0 (12.45)[a]	>25.0 (9.45)	>25.0 (6.54)
15	**miltefosine**[b]	8.78 ± 0.41	10.60 ± 0.46	N.D.
16	**glucantime**[b]	32.00 ± 1.78	N.D.	N.D.
17	**nifurtimox**[c]	N.D.	N.D.	**7.7 ± 0.5**

[a]PGI: percentage growth inhibition of the parasite cell, determined at 25 μM. [b]Leishmanicidal reference. [c]Anti-Chagasic ref 36. Note: parameters marked in bold indicate a pronounced antiparasite activity. N.D.: not determined.

With all these arguments, herein we designed a series of new 2-arylquinazolin-4-hydrazine derivatives, where the hydrazine moiety is connected to an electron-deficient heterocycle, the 2-arylquinazoline, with a demonstrated anti-trypanosomatid activity against *Leishmania* parasites.[32]

RESULTS AND DISCUSSION

Design and Synthesis. The design of the target 2-arylquinazolin-4-hydrazines **3a−k** was inspired by a series of active 2-arylquinazolin-4(3*H*)-ones, which showed remarkable leishmanicidal activity against *Leishmania* parasites with the ability to interfere with the parasite folate metabolism.[32] Herein, we replaced the oxygen atom by a hydrazine moiety at 4-position of the 2-arylquinazoline core to generate a dual-targeting system: (i) NO released by the in situ oxidation of the hydrazine moiety placed in the electron-deficient quinazoline ring and (ii) the antifolate pathway by the 2-arylquinazoline core (Chart 1). The selection of functionalities for the designed 2-arylquinazolines **3a-k** (Scheme 1) was focused on those aryl functionalities that led to the best activity/toxicity profile in the 2-arylquinazolin-4(3*H*)-ones: 4-Cl-, 3-OMe-, and 4-F-phenyl.[32] Other 3-chlorophenyl (**3f**) or 3-bromophenyl (**3g**) electron-deficient aryl functionalities also were considered in order to construct compounds consisting of an electron-deficient ring connected to a hydrazine group, which is convenient for the decomposition of the hydrazine moiety.[16−19] Also, we prepared a 6-chloro-substituted derivative (**3j**), but the scaffold was not explored by its low solubility.[32,33]

The preparation of 2-arylquinazolin-4-hydrazines **3a−k** was performed from their corresponding 2-arylquinazolin-4(3*H*)-ones **1a−k**[33] through a sequential two-step reaction (Scheme 1).[34,35] First, **1a−k** were reacted with phosphorus oxychloride to give the corresponding 2-aryl-4-chloroquinazolines **2a−k**, which were sufficiently pure for the next reaction step. They were reacted with hydrazine in ethanol to give the desired 2-arylquinazolin-4-hydrazine **3a−k** in excellent yields (83−91%). A second group of phthalazine-hydrazines **4a**, **4b**, and **4c** (Table 1) were prepared previously from phthalazin-1,4-dione[34,35] to complement our structural comparisons. Experimental details and spectroscopic information for pure

https://doi.org/10.1021/acsomega.2c06455
ACS Omega 2022, 7, 47225−47238

Table 2. Cytotoxicity, *Leishmania* Antiamastigote Activity, and Selectivity Indexes of Active Derivatives 3a−f

	compounds	peritoneal macrophage, CC_{50} (μM)	J774.1A macrophage, CC_{50} (μM)	amastigote, IC_{50} (μM) *L. braziliensis* ($S.I._{Leishmania}$)[a]	epimastigote, IC_{50} (μM) *T. cruzi* ($S.I._{T.cruzi}$)[b]
1	**3a**	61.02 ± 2.34	90.20 ± 4.32	8.26 ± 0.45 (7.4)	<3.6
2	**3b**	**>100.0**	**>120.00**	**7.41 ± 0.39 (>13.5)**	>6.7
3	**3c**	**89.86 ± 3.77**	**104.78 ± 5.66**	**8.96 ± 0.53 (10.0)**	**9.1**
4	**3d**	77.98 ± 3.89	78.59 ± 3.99	12.67 ± 0.78 (6.2)	5.5
5	**3e**	84.76 ± 3.67	114.58 ± 5.43	13.99 ± 0.89 (6.1)	6.4
6	**3f**	**>100.0**	**>120.0**	**8.43 ± 0.51 (>11.9)**	no active
7	**miltefosine**	**67.78** ± 3.11	**72.34** ± 3.45	**21.23** ± 1.13 (3.2)	
8	**glucantime**	138.22 ± 10.11		12.21 ± 2.12 (11.3)	
9	**nifurtimox**		280.0 ± 4.00[c]		36[c]

[a]Selectivity indexes calculated from ratio between the CC_{50} (peritoneal macrophage) and IC_{50} (amastigotes of *L. braziliensis*). [b]Selectivity indexes calculated from the ratio between the CC_{50} (J774.1A) and IC_{50} of epimastigotes (*T. cruzi*). [c]From ref 36.

compounds can be found in the Supporting Information. A comparative analysis based on NMR spectra and theoretical calculations revealed that the compound is under the tautomeric form: (*Z*)-1-(2-phenylquinazolin-4(3*H*)-ylidene)-hydrazine. A detailed discussion can be found in Section S2 of the Supporting Information. Table S1 shows clearly that the imine-tautomer is energetically more accessible than the hydrazine-tautomer.

Biological Evaluation. All synthesized compounds were initially tested against promastigotes of *L. braziliensis* and *L. infantum* and against epimastigotes of *T. cruzi* (Table 1). In general, the compound showed a higher activity against *Leishmania* than against *T. cruzi*. Against *Leishmania*, it should be noted that some 2-arylquinazolin-4-hydrazines exhibited a higher activity against than miltefosine and glucantime references. In general, compounds were barely more active against *L. infantum* parasite than against *L. braziliensis*. Six of them (**3a**, **3b**, **3c**, **3d**, **3e**, and **3f**) displayed low-micromolar IC_{50} values ranging from 3.85 to 10.06 μM and from 1.20 to 12.67 μM against *L. braziliensis* and *L. infantum*, respectively. Curiously, the derivative **3e** showed the highest activity against promastigotes of *L. infantum* with an IC_{50} value of 1.2 μM and a discrete activity against *L. braziliensis* (IC_{50} = 10.06 μM). In contrast, compound **3h** was active against *L. braziliensis* (12.21 μM) but inactive against *L. infantum*. Meanwhile, the quinazolines **3g** (3-Br-phenyl) and **3j** (X, Y= Cl displayed discrete responses against both *Leishmania* strains, whereas **3i** did not show activity. The latter may be mainly attributed to its poor solubilities. Interestingly, the active compounds **3c**, **3d**, and **3e** were significantly more active than their corresponding 2-arylquinazolin-4(3*H*)-one parent compounds against promastigote *Leishmania* parasites,[32] which puts in evidence that the incorporation of the hydrazine moiety enhances the potency of the 2-arylquinazoline as leishmanicidal.

Regarding *T. cruzi* activity, derivatives **3b**, **3c**, **3d**, and **3e** showed the best anti-epimastigote activities with IC_{50} values of 17.95, 11.48, 14.32, and 17.99 μM, respectively. Similar to antileishmanial response, compounds **3g** to **3j** demonstrated modest responses against *T. cruzi*. The active compounds against *Leishmania*, **3a** and **3f**, showed weak anti-*T. cruzi* activities with PGI values of 42.7 and 38% at 25 μM, respectively. The rest of the derivatives displayed PGI magnitudes less than 22% at 25 μM, except **3j** (PGI = 37.7%). The 2-arylquinazolin-4-hydrazines were less active than nifurtimox by two- to threefold. As an anti-*T. cruzi* agent, it should be noted that 2-arylquinazolin-4-hydrazines bearing electron-withdrawing moieties at 4-position of the aryl ring (e.g., 4F, 4Cl, and 4Br) were the most active compounds. Compound **3e** (4-Me-phenyl) exhibited an activity comparable to electron-deficient derivatives **3c** and **3d**. Compounds **3h** and **3i** were also poorly active. On the other hand, against both parasites, the phthalazin-hydrazine, **4a**, **4b**, and **4c**, they did not show antitrypanosomal activities (PGI < 20%). It reflects the fact that the 2-arylquinazoline was a more convenient scaffold than phthalazine to design hydrazine derivatives, and the incorporation of the electron-withdrawing aryl moiety is preferred to generate active antitrypanosomal agents.

Next, the most active compounds (**3a−3f**) were selected for cytotoxic evaluation using (i) primary peritoneal macrophages[32,35] and (ii) J774.1A macrophages[36] (Table 2). The 2-arylquinazolin-4-hydrazines **3b** and **3f** were identified as the least toxic compounds with CC_{50} values higher than 100 μM against both macrophage lines. Derivatives **3c** and **3e** displayed CC_{50} of 104.78 and 114.58 μM against J774.1A macrophages, respectively, and CC_{50} values of 89.86 and 84.76 μM against peritoneal macrophages, respectively. Meanwhile, compounds **3a** and **3d** were recognized as the most toxic agents among the studied active 2-arylquinazolin-4-hydrazines, CC_{50} values ranging from 60 to 90 μM.

Then, we evaluated the potential of these six compounds against infective intracellular amastigotes of *L. braziliensis*.[32] Compounds **3a**, **3b**, **3c**, and **3f** showed the best antiamastigote activity having IC_{50} values between 7.41 and 8.96 μM against *L. braziliensis*, whereas compounds **3d** and **3e** displayed good IC_{50}, 12.67 and 13.99 μM, respectively. The antiamastigote activity of the compounds **3b**, **3c** and **3f** were barely higher than that found for glucantime reference (IC_{50} = 12.21 μM). Then, selectivity index (S.I.) values relative to *Leishmania* were calculated as the ratio of the CC_{50} value of the macrophage (peritoneal) to IC_{50} of amastigotes of *L. braziliensis*. Derivatives **3b**, **3c**, and **3f** showed the best S.I., with values higher than 10, which is in the same range compared to glucantime and better than miltefosine S.I. All six derivatives displayed higher antiamastigote activity and selectivity than miltefosine. The rest of the compounds, **3a**, **3d**, and **3e**, showed S.I. values between 6.1 and 7.5. On the other hand, as an anti-*T. cruzi* agent, the compounds **3b−3e** showed S.I. values higher than 5.5 (Table 2). Compound **3a** displayed an S.I. lower than 3.6, with nifurtimox (S.I. = 36) being more selective than quinazolin-hydrazines.[36]

Drug-like Profiles. First, drug-like properties for active compounds **3b**, **3c**, and **3f** were studied in silico using the Swiss-ADME platform.[37] Physicochemical properties (lipophilicity, water solubility, pharmacokinetic properties, and

https://doi.org/10.1021/acsomega.2c06455
ACS Omega 2022, 7, 47225−47238

Table 3. In Silico Physicochemical, Pharmacokinetic, and Drug-likeness Parameters of 3b, 3c, and 3f

type of parameter	parameter	3b	3c and 3f
physicochemical properties	M.W. (g/mol)[a]	254.26	270.72
	N° rotatable bonds	2	2
	N° H-bond acceptors	4	3
	N° H-bond donors	2	2
	molar refractivity	72.14	77.19
	TPSA (Å^2)[b]	63.83	63.83
lipophilicity	log $P_{o/w}$ (iLOGP)	2.35	2.07
	log $P_{o/w}$ (XLOGP3)	3.18	3.71
	log $P_{o/w}$ (WLOGP)	2.95	3.05
	log $P_{o/w}$ (MLOGP)	3.19	3.31
	log $P_{o/w}$ (SILICOS-IT)	2.33	2.55
	consensus log $P_{o/w}$	2.80	2.94
water solubility	log S (ESOL)	−3.91	−4.35
	solubility	123 μM (soluble)	45 μM (moderately soluble)
	log S (Ali)	−4.19	−4.74
	solubility	64.3 μM (moderately soluble)	18.1 μM (moderately soluble)
pharmacokinetic properties	GI absorption[c]	high	high
	BBB permeant[d]	yes	yes
	P-gp substrate[e]	no	no
	CYP1A2 inhibitor	yes	yes
	CYP2C19 inhibitor	yes	yes
	CYP2C9 inhibitor	no	no
	CYP2D6 inhibitor	no	no
	CYP3A4 inhibitor	no	no
	log K_p (skin permeation)	−5.59 cm/s	−5.32 cm/s
drug-likeness	Lipinski	fit; 0 violation	fit; 0 violation
	Ghose	fit	fit
	Veber	fit	fit
	Egan	fit	fit
	Muegge	fit	fit
	bioavailability score	0.55	0.55
medicinal chemistry	PAINS	0 alert	0 alert
	Brenk	1 alerts: hydrazine	1 alert: hydrazine
	lead-likeness	fit	do not fit; 1 violation: XLOGP3 > 3.5

[a]MW: molecular weight. [b]TPSA: topological polar surface area. [c]G.I.; gastrointestinal. [d]BBB: blood−brain barrier. [e]P-gp: P-glycoprotein. Drug-likeness maps are found in Figure S3.

other drug-likeness predictors) are summarized in Table 3. In general, the compounds showed good physicochemical properties within Lipinsky,[38] Ghose, Veber, Egan, and Muegge rules.[39] Meanwhile, the compounds displayed a good aqueous solubility (from 43 to 125 μM), which is in good concordance with the appreciable solubility of the compounds **3b**, **3c**, and **3f** in culture. Within the pharmacokinetic properties, compounds showed high G.I. (gastro-intestinal) indexes, positive BBB (blood brain barrier) permeabilities, good skin permeation (Log K_p by about −5.3/−5.6 cm/s), and a negative substrate for P-gp. Compounds showed to be potential substrates for CYP1A2 and CYP2C19 proteins but not for the CYP2C9, CYP2D6, and CYP3A4 proteins. Within medicinal chemistry, no PAINS moieties were identified from the 2-arylquinazolin-4-hydrazine, and only an alert was indicated for the hydrazine. To support this, we passed the three compounds through a filter for recognizing PAINS,[40] and none of them represent a PAINS. Finally, to evaluate the security of the compounds, we performed the Ames test to discard the mutagenic effect derived from the interaction of compounds with biological systems. The mutagenic assay was performed using a genetically modified *Salmonella Typhimurium* TA 98 for the compound **3c**.[41] From the Ames test, compound **3c** was identified as a non-mutagenic agent due to the fact that it was not able to at least double the number of colonies of spontaneous revertant colonies (0.0 μg/plate of compound) for at least two consecutive dose levels,[41] while revertant colonies were obtained with the mutagenic 4-nitro-*o*-phenylenediamine (NPD) positive control (Table 4). Thus, the hydrazine connected to 2-arylquinazolin at 4-position emerges as a safe pharmacophore from the toxic and mutagenic point of view.

Mechanism of Action Studies. Herein, we focused on validating (i) antifolate activity and (ii) NO production via

Table 4. Ames Results in TA 98 Strain

comp.	doses (μg/plate)	revertants number	conclusion
3c	0.0	8.5 ± 2.5	no mutagenic
	27.9	8.0 ± 2.0	
	37.2	4.5 ± 2.0	
	55.8	5.0 ± 0.5	
	111.7	8.0 ± 1.0	
	335.0	9.5 ± 0.5	
positive control (NPD)	20.0	394.0 ± 10	mutagenic

https://doi.org/10.1021/acsomega.2c06455
ACS Omega 2022, 7, 47225−47238

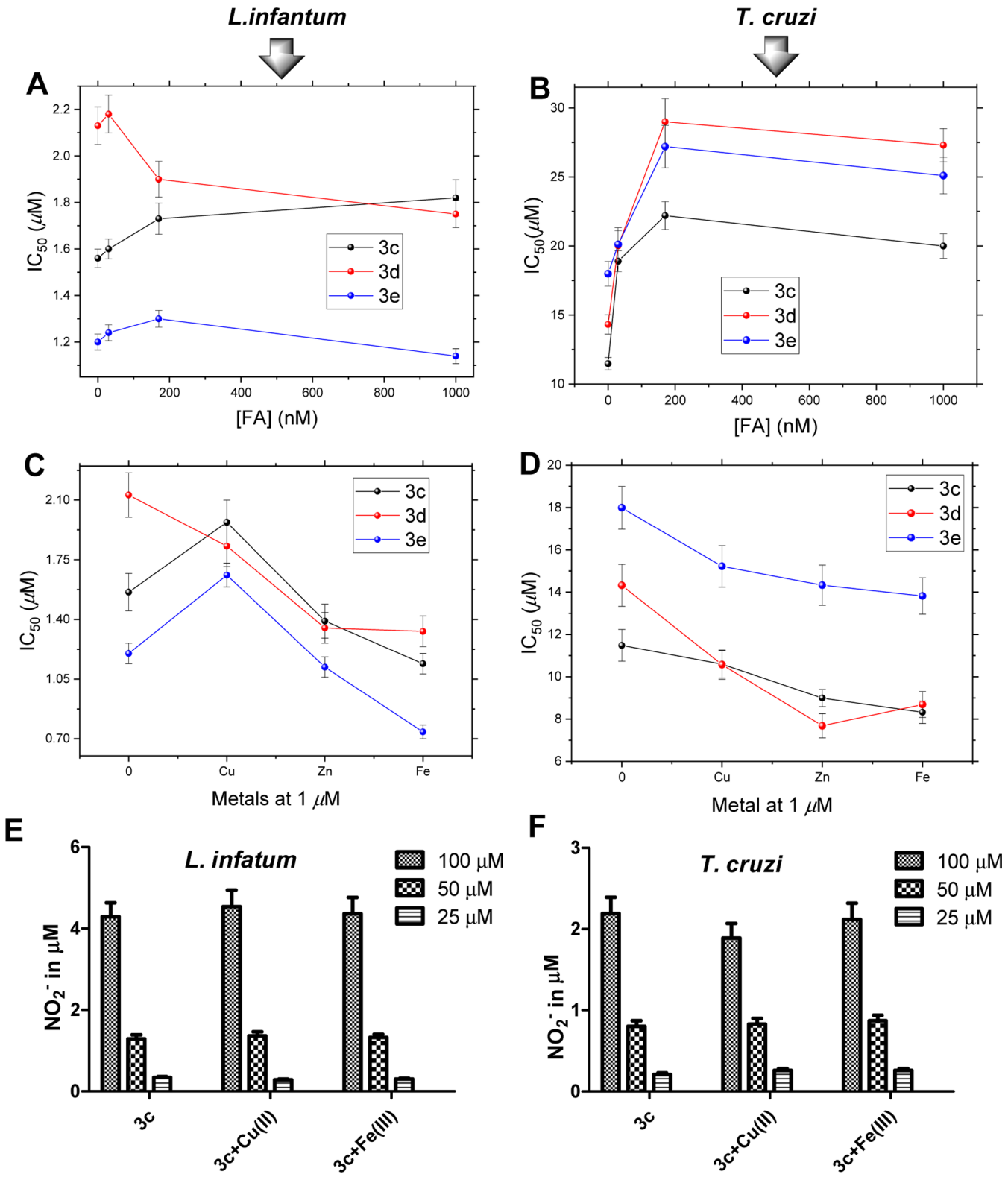

Figure 2. In vitro efficacy (IC_{50}) of **3c**, **3d**, and **3e** on promastigotes of *L. infantum* (A) and epimastigotes of *T. cruzi* (B) in the absence and presence of FA. In vitro efficacy (IC_{50}) of **3c**, **3d**, and **3e** for *L. infantum* promastigotes (C) and *T. cruzi* epimastigotes (D) in the absence and presence of Cu(II), Fe(III), and Zn(II) cations. Concentrations of the nitrite ion (in μM) from treated *L. infantum* promastigotes (E) and *T. cruzi* (F) epimastigotes with **3c**.

oxidative decomposition of the hydrazine moiety. Regarding the antifolate pathway, there are many quinazoline derivatives based on that mechanism.[42] From an indirect strategy,[32] we evaluated the antifolate activity of the compounds **3c**, **3d**, and **3e** through the measurement of IC_{50} against axenic parasites in the presence or absence of D,L-folic acid (FA) (Figure 2A,B). If an antifolate activity is involved in the anti-trypanosomatid activity of the 2-arylquinazolines, an increase in the IC_{50} of the

https://doi.org/10.1021/acsomega.2c06455
ACS Omega 2022, 7, 47225−47238

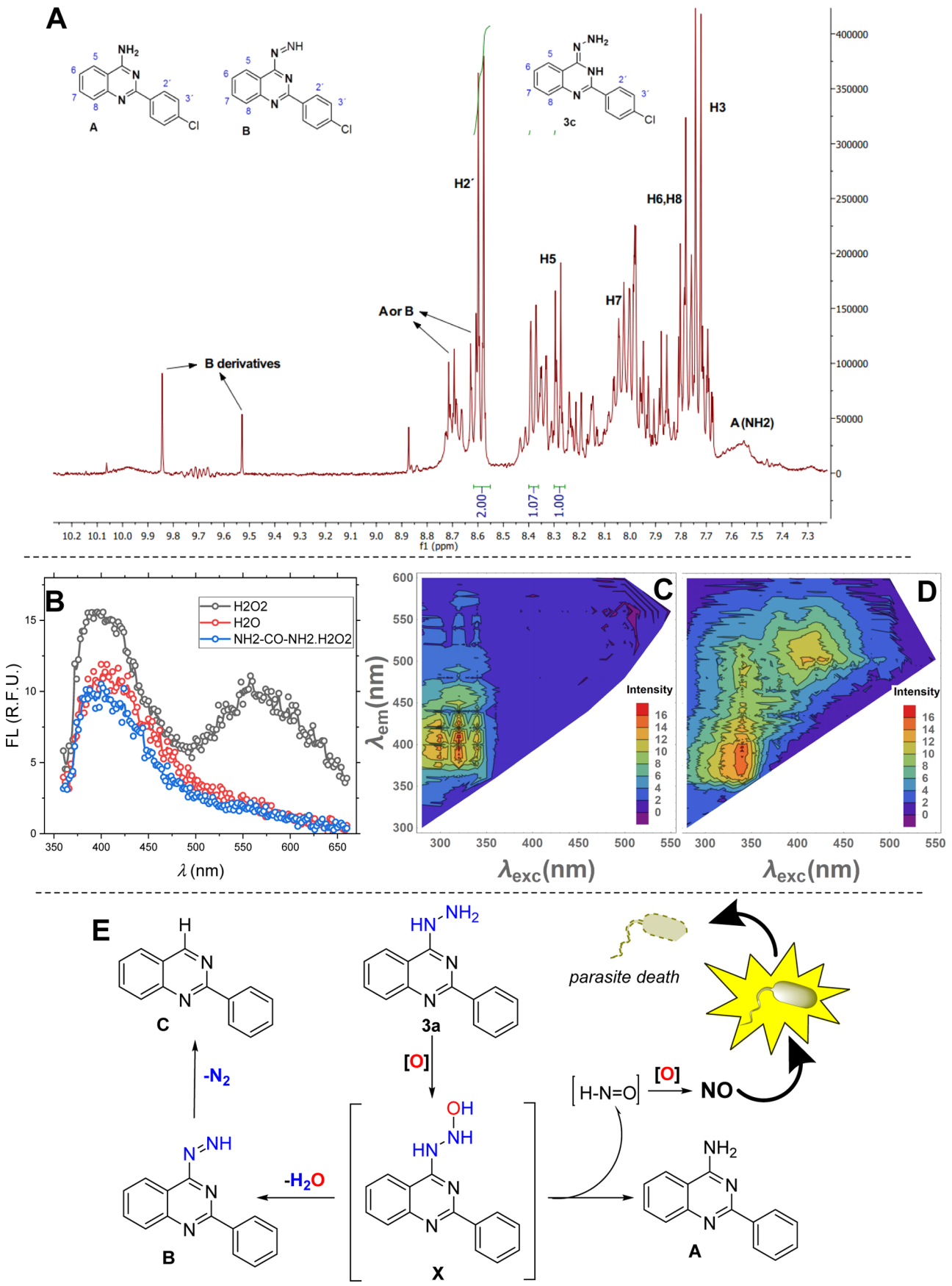

Figure 3. (A) ^{1}H-NMR spectrum for solution of **3c** after 2 weeks of incubation with H_2O_2; (B) emission spectra of **3h** in the absence and presense of the oxidant (H_2O_2 or $NH_2CONH_2{\cdot}H_2O_2$); emission-excitation matrix (EEM) plot for **3h** in the absence (C) and presence (D) of H_2O_2; and (E) tentative proposal for the decomposition of hydrazine in 2-arylquinazolin-4-hydrazine (**3a**) to release NO.

https://doi.org/10.1021/acsomega.2c06455
ACS Omega 2022, 7, 47225−47238

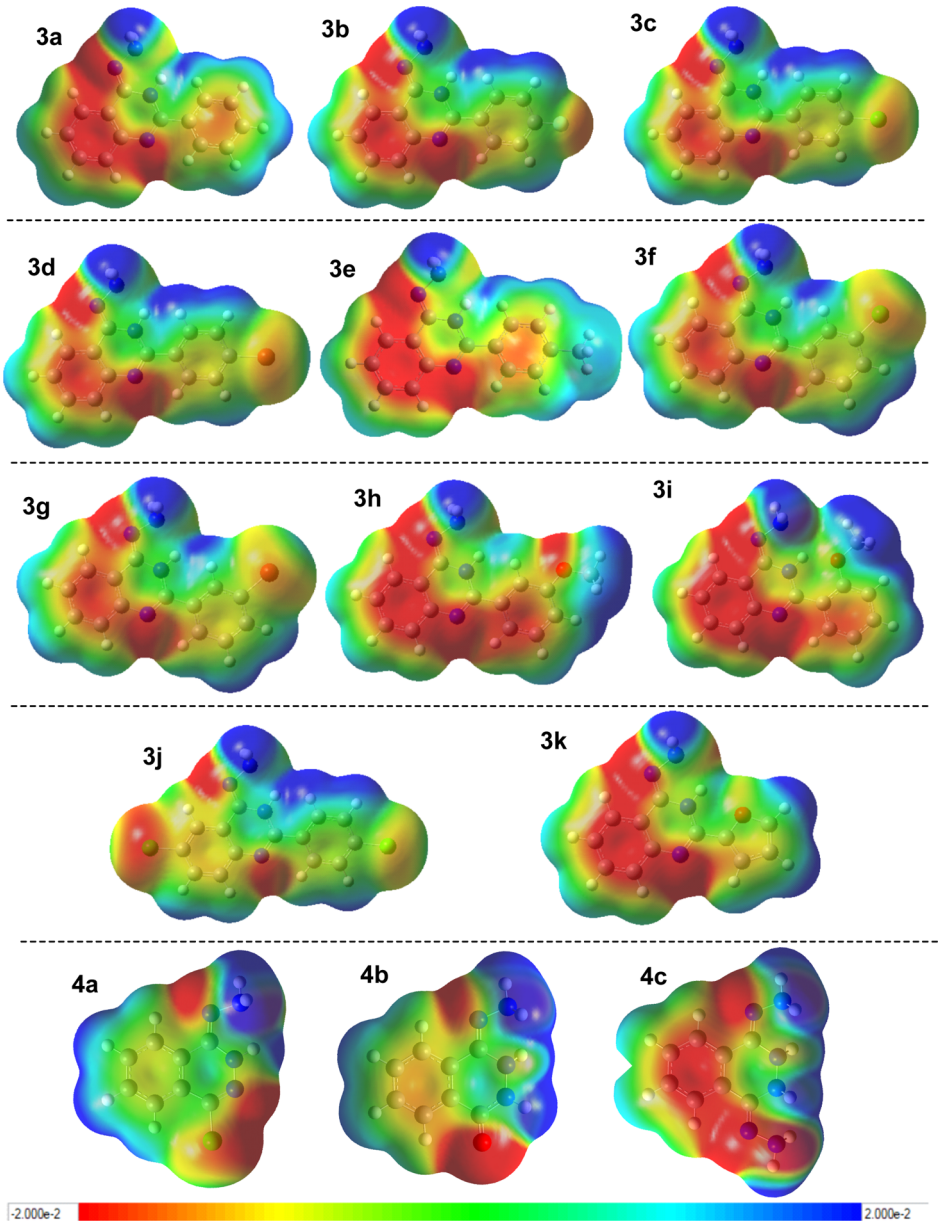

Figure 4. Electrostatic potential surface (EPS) for the 2-arylquinazolin-4-hydrazine **3a**−**k** and phthalazin-1-hydrazines **4a**−**c**.

derivatives in the presence of FA is expected.[32] Increasing IC_{50} values by about twofold were found with the addition of FA for treated epimastigote *T. cruzi* with **3c**, **3d**, and **3e** (Figure 2B). In contrast, the presence of FA displayed a modest increase in IC_{50} for treated *Leishmania*, in particular, for **3c** (Figure 2A). Conversely, IC_{50} of miltefosine and nifurtimox was not affected by the addition of FA to the treated parasites. Then, we concluded that the antiepimastigote response of **3c**, **3d**, and **3e** could be derived from an antifolate activity, whereas the significant leishmanicidal activity of them seems to be attributed primarily to an alternative mechanism, the antifolate activity being a secondary mechanism for *Leishmania*.

Next, we explored the role of the NO production in the antitrypanosomatid activity of active 2-arylquinazolin-4-hydrazines. Furthermore, we studied the effect of some polyvalent transition metals (Fe^{3+},Cu^{2+}, and Zn^{2+}) in the biological activity and modulation of NO release. For them, we performed separately four experiments: (i) anti-trypanosomatid activity of **3c**, **3d**, and **3e** in the presence of transition metallic cations; (ii) NO-production in treated parasites in the absence and presence of metallic cations; (iii) tentative decomposition of the hydrazine moiety in **3c** or **3h** through spectroscopic experiments; and (iv) theoretical study based on the HOMO−LUMO orbitals and electrostatic potential surface (EPS) to distinguish the oxidation ability of the hydrazine moiety.

Due to the high susceptibility of the hydrazine moiety connected to the electron-deficient ring to the oxidation in the presence of transition metals,[17−19] we first evaluated the effect of the metal cations (at 1 μM) on cell viability of **3c**-, **3d**-, and **3e**-treated parasites (Figure 2C,D). In general, a moderate decrease in IC_{50} values, mainly upon Zn^{2+} and Fe^{3+}, was found for all treated parasites in the presence of transition metals. Only Cu^{2+} displayed an increase in IC_{50} values in *Leishmania* parasites for 3c and **3e**.

With this information, we measured the level of nitrite ions in parasite culture by the Griess test for non-infective *L. infantum* and *T. cruzi* in the presence or absence of the most

https://doi.org/10.1021/acsomega.2c06455
ACS Omega 2022, 7, 47225−47238

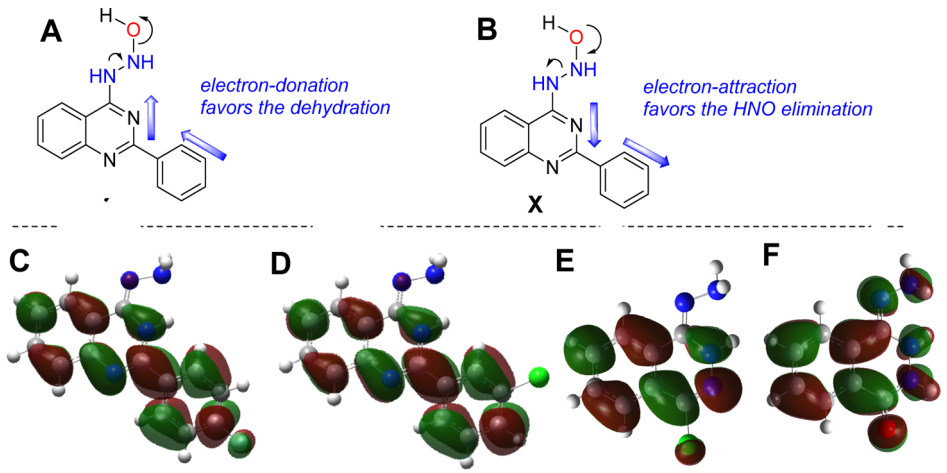

Figure 5. Tentative mechanistic dehydration (A) and HNO-elimination (B) in intermediate **X** from an electronic point of view and LUMO maps for **3c** (C), **3f** (D), **4a** (E), and **4c** (F).

active compound **3c** at different doses (Figure 2E,F).[34] Further measurements in the presence of Cu^{2+} and Fe^{3+}cations were performed to study whether transition metals mediated NO production. A control experiment was performed with the 2-(4-chlorophenyl)quinazolin-4(3*H*)-one, which was active against *Leishmania* parasites,[32] in order to discard a direct mediation by the chemical system to activate the nitric oxide synthase (NOS) enzyme. From results, treated parasites displayed an appreciable amount of nitrite ion in sub-micromolar ranges, and its production showed dependence with the compound doses. No production was detected in the presence of the 2-(4-chlorophenyl)quinazolin-4(3*H*)-one, which suggests that the NO is possibly not generated from an enzymatic stimulation of the chemical system, opening the door to the role of the decomposition of hydrazine moiety to interpret the NO in the 2-arylquinazolin-4-hydrazine. Interestingly, *Leishmania* parasites showed a more significant nitrite ion production than *T. cruzi* under the same conditions. The use of Cu^{2+} and Fe^{3+} cations increases discretely the nitrite ion concentration. This evidence suggests that the 2-arylquinazolin-4-hydrazines could be involved in the production of NO within parasites, and it could be attributed to chemical decomposition of hydrazine to NO and organic sub-products. Meanwhile the cations improved, discretely, the activity of the active compounds, but they did not seem to play an essential role in the NO production, its mediation being discarded in hydrazine decomposition.

To demonstrate that the production of NO in treated parasites was derived from the partial chemical decomposition of 2-arylquinazolin-4-hydrazine, we performed spectroscopic studies (NMR and fluorescence) in the absence and presence of an oxidant (H_2O_2 or $NH_2-CO-NH_2{\cdot}H_2O_2$) (Figure 3). The NMR experiment confirmed that compound **3c** was decomposed in at least three additional products: 4-amino-2-arylquinazoline (A), 1-(2-arylquinazolin-4-yl)diazene (B), or 2-arylquinazoline (C) (Figures 3A, S1, and S2). A single peak by about 9.6 or 9.7 ppm may be associated to the (−N═NH) proton in metabolite B, while a broad peak at 7.5 ppm may belong to the amino proton in metabolite A. Specific peaks at 8.34 and 7.8 ppm are reported in the literature for 4-aminoquinazolines.[43] To support this evidence, we performed a fluorescence study for the resulting solution, and it was compared with that solution in the absence of an oxidant. It is documented that 2-aminoquinazolines present fluorescence properties with a normal emission at 400−430 nm and a secondary anomalous at 575−600 nm.[44−46] It is well known that the fluorometry is a high-sensitivity technique, which facilitated the detection of low-concentration compounds. From the fluorescence experiment, in general, all 2-arylquinazolin-4-hydrazines showed a maximum normal emission wavelength at 400 nm (Figures 3B−D and S8 and S9). Under oxidative conditions, only the compound **3h** showed an emission spectrum with appreciable changes, being our model structure. The emission spectrum of **3h** showed the emergence of an additional anomalous emission peak at 575 nm (Figure 3B). To facilitate the identification of the anomalous emission band, an emission-excitation matrix (EEM) plot[47] was performed, and the anomalous emission band (575 nm) in combination with the normal emission band was confirmed for the compound **3h** upon oxidative conditions. Meanwhile, only the normal emission band was seen in the absence of the oxidant (Figure 3C,D). The latter supports the formation of product A, and the solution must consist of a mixture between starting quinazoline and the metabolite A. UV−vis spectroscopy did not allow the detection of the low decomposed products (Figure S5F). With all this biological and chemical evidence, we proposed a tentative decomposition pathway for the hydrazine moiety in 2-arylquinazolin-4-hydrazine with NO releasing from parasite culture (Figure 3E). Initially, 2-arylquinazolin-4-hydrazine is oxidized within parasites to form intermediate **X**. Subsequently, **X** may suffer: (i) a dehydration leading B and (ii) a decomposition of the hydroxylhydrazinyl moiety to form product A and H−NO. This last species could be oxidized to NO through the Fe(II)$-O_2$ complex, which is present in the SOD enzyme of trypanosomatids.[48]

In order to understand theoretically the origin of the tentative decomposition of the hydrazine moiety in 2-arylquinazolin-4-hydrazine, we analyzed its HOMO−LUMO and EPS. From EPS (Figure 4), it should be noted primarily that the imine-tautomer presented a more negative electron density on bonded nitrogen (more red color in EPS map) to the heterocyclic ring than hydrazine-tautomer; thus, the imine-tautomer is more suitable to suffer oxidation than the hydrazine-tautomer in the studied 2-arylquinazoline/phthalazin-hydrazines (compare Figure 4 vs Figure S14). Comparison

https://doi.org/10.1021/acsomega.2c06455
ACS Omega 2022, 7, 47225−47238

between the 2-arylquinazolin with phthalazin-hydrazines showed that the first presented a more negative bonded nitrogen to the heterocyclic ring than the phthalazine analogue, although these differences are smaller, which supposes a higher nucleophilic character in the terminal amino of hydrazine of 2-arylquinazoline than in the phthalazine-hydrazine. It is highly required to form metabolite **X** (Figure 3E). Thus, from the electronic point of view, the nucleophilic addition of the amino terminal to the oxidant for the formation of **X** is more favored in the 2-arylquinazolin-hydrazine than phthalazin-hydrazines. Within the 2-arylquinazolin-4-hydrazines, no appreciable differences were noted from the electronic density point of view, but some important differences were noted on the quinazoline core. A lower electron density was seen on the benzo-core of the 2-arylquinazoline bearing the electron-deficient aryl moiety (**3b**, **3c**, **3d**, **3f**, **3g**, and **3j**) than on those bearing the electron-rich moiety (**3a**, **3e**, **3h**, **3i** and **3k**). The electron-deficient nature of the quinazoline core could be an important electronic feature to favor the decomposition of **X** to form A with release of HNO because this transformation mechanistically required that the quinazoline core acts as an electron acceptor. It favors the electronic movement from the hydroxyl moiety to bonded nitrogen to form H−NO (Figure 5A). In contrast, a higher electronic density on the quinazoline core was given to the system in an electron donor to favor the dehydration of **X** via an electron movement from pyrimidyl to the hydrazine moiety (Figure 5B). From HOMO−LUMO, LUMO maps showed that an electron transfer (ET) from the heterocyclic core to the hydrazine moiety is more suitable in the phthalazine-hydrazine than in the 2-arylquinazolines (Figures 5C−F and S6−S13), supporting the fact that the 2-arylquinazoline is a more convenient scaffold to favor the required electronic movement from hydrazine to the quinazoline ring for decomposition of hydrazine to release HNO (Figure 5A,B). Further HOMO−LUMO data and graphical orbitals can be found in the Supporting Information.

In summary, we showed the potential of a hydrazine as a pharmacophore for the construction of a new type of antitrypanosomal agent based on its feasible oxidative decomposition to release NO in electron-deficient systems and the high toxicity of this small molecule against trypanosomatids. Then, a series of 2-arylquinazolin-4-hydrazines were synthesized, and some of the derivatives, **3b**, **3c**, and **3f**, showed a good in vitro activity against non-infective and infective strains of *Leishmania* and against non-infective strain of *T. cruzi*, lower cytotoxicity against different macrophages, high selectivity indexes over 10 units, and non-mutagenic effects. Interestingly, studies of the mechanism of action suggested that the production of NO could be one of the responsible anti-trypanosomatid activities of the 2-arylquinazolin-4-hydrazines, in combination with a discrete contribution of antifolate activity. Chemical experiments based on spectroscopic measurements identified that the formation of the subproduct under oxidative environments in conjunction with biological NO releasing from treated parasites allowed us to propose a mechanistic decomposition of the hydrazine moiety to form NO. Finally, theoretical calculations based on HOMO−LUMO and EPS analysis showed that the feasible oxidative decomposition of the hydrazine moiety in 2-arylquinazolines depended on two electronic conditions: (i) to guarantee a high electron density on the bonded nitrogen of the hydrazine moiety and, at the same time, (ii) a strong electron attraction from hydrazine to the heterocyclic ring with a non-ET process. It was consistently achieved for the 2-arylquinazolin-4-hydrazine over, for example, phthalazin-1-hydrazine, and it showed to be modulated by the incorporation of electron-deficient aryl moieties. All the evidence allowed us to explain the significant biological activity of the electron-aryl-deficient 2-arylquinazolin-4-hydrazine, and our investigation opens a new perspective for the design of effective and safe NO-donors with anti-trypanosomatid activities.

METHODS

General Chemistry. 2-Arylquinazolin-4(3*H*)-ones **1a−k** were previously prepared.[32] The rest of the reagents were purchased from commercial sources and used without further purification. Solvents were anhydrous HPLC grade. ^{1}H NMR and ^{13}C NMR spectra were recorded on a 400 MHz NMR-spectrometer (Bruker-400) or 250 MHz NMR-spectrometer JEOL. Multiplicity is indicated as follows: s (singlet), d (doublet), t (triplet), m (multiplet), dd (doublet of doublets), and brs (broad singlet); chemical shifts were measured in parts per million (δ), and coupling constants (J) are given in Hz. Proton chemical shifts were given relative to tetramethylsilane (δ 0.00 ppm) in $CDCl_3$ or DMSO-d_6. Carbon chemical shifts are internally referenced to the deuterated solvent signals in $CDCl_3$ (δ 77.00 ppm) or DMSO-d_6 (δ 40.02 ppm). Elemental analyses of the synthesized compounds were performed using a PerkinElmer 2400 CHN analyzer: results fell in the range of 0.4% of the required theoretical values. TLC was performed using commercially available 100−400 mesh silica gel plates (GF254) and visualized under UV light (at 254 nm). Absorption and fluorescence spectral data were obtained from a Thermo Scientific Varioskan Flash Multimode instrument for air-equilibrated solutions at 25 °C. EEM plots were obtained as described previously (Figures S4 and S5).[47]

General Procedure for Synthesis of 2-Arylquinazolin-4-hydrazines. The corresponding starting materials **1a−k** (0.5 mmol, 1.0 equiv) were mixed with $POCl_3$ (6 equiv) according to the reported protocol with a few modifications.[34,35] The reaction mixture was stirred for 4−6 h at 100 °C. It was monitored by TLC. The reaction mixture was quenched with water at 0 °C with dichloromethane (3 × 20 mL). The combined organic extracts were washed with saturated aqueous NaCl solution, dried over anhydrous Na_2SO_4, and filtered. The mixture was passed by a flash chromatographic column to obtain the intermediates **2a−k**. The isolated product was used for the next reaction step. Then, to a hot hydrazine hydrate (4 equiv) solution in ethanol was added the intermediates **2a−k** (1 equiv) at 0.1 M concentration and heated at 70 °C for 2 h. The reaction was monitored by TLC. The reaction mixture was cooled at 0 °C, and then, the resulting solid was filtered by vacuum to give from a pale yellow to orange solid. The isolated solid was recrystallized with cold ethanol to yield the pure product. The product were characterized by NMR spectroscopy. Detailed spectroscopic data and spectra can be found in the Supporting Information.

In Vitro Anti-*T. cruzi* Evaluation on Epimastigotes. The effect of the studied compounds on the epimastigote viability of *T. cruzi* (CL Brener clone) was determined through the turbidimetric technique.[36] Stock solutions (at 3000 μM) of the tested compounds in DMSO were prepared. Fresh solutions were diluted in the culture medium to obtain the different concentrations from 0.5 to 25 μM. All controls and tested well contain no more than 1% of DMSO. The screening

https://doi.org/10.1021/acsomega.2c06455
ACS Omega 2022, 7, 47225−47238

was performed in 24-well microliter plates maintained at 25 °C. Briefly, 2×10^6 parasites/mL were exposed to increasing concentrations from 0.5 to 25.0 μM (1.0, 5.0, 10.0, 20.0, and 50.0 μM) of each compound for 120 h at 25 °C. The biological effect of these compounds was evaluated through absorbance measurements at 595 nm using a spectrometer El301 microwell at 5 days. Untreated control parasites were used to calculate the relative proliferation. Nifurtimox was used as a reference drug. The percentage of growth inhibition (PGI) was determined as follows: PGI (%) = $\{1 - [(A_p - A_{0p})/(A_c - A_{0c})]\} \times -100$, where $A_p = A_{595}$ of the culture containing the compound at day 5; $A_{0p} = A_{595}$ of the culture containing the compound at day 0; $A_c = A_{595}$ of the culture in the absence of any drug (control) at day 5; and $A_{0c} = A_{595}$ in the absence of any drug at day 0.

To determine IC_{50} values, PGI was followed of increasing concentrations of the corresponding agent. The IC_{50} was taken as the concentration of the agent needed to reduce the PGI to 50%.

In Vitro Anti-*Leishmania* Evaluation on Promastigotes. The cell viability of 2-aryl-quinazolin-4-hydrazines **3a**−**k** on *Leishmania infantum* (MHOM MA67I7MAP263) strain was assessed using the 3-(4,5-dimethylthiazol-2-yl)-2,5-diphenyltetrazolium bromide (MTT) assays with a few modifications.[34] Stock solutions (at 3000 μM) of the tested compounds in DMSO were prepared. Fresh solutions were diluted in the culture medium to obtain the different concentrations from 0.5 to 25 μM. All controls and tested well contain no more than 1% of DMSO. The screening was performed in 96-well microliter plates maintained at 25 °C. Briefly, 2×10^6 parasites/mL were exposed to increasing concentrations from 0.5 to 25.0 μM (1.0, 5.0, 10.0, 20.0, and 50.0 μM) of each compound for 72 h at 25 °C. Controls contain 1% of DMSO and medium. After incubation, cells were treated with 100 μL 0.4 mg/mL MTT for 4 h at 37 °C. Subsequently, the medium was removed, and 100 μL of DMSO was added to the resulting mixture to dissolved formazan salt. The solubilized formazan product was quantified through absorbance measurements at 570 nm using a Thermo Scientific Varioskan Flash Multimode instrument at 72 h. Miltefosine and glucantime were used as reference drugs. Untreated control parasites were used to calculate the relative proliferation. The percentage of parasite inhibition with regard to controls was calculated as = 100 − [(parasite counts in treated cells/parasite counts in untreated cells) − 100].

Ex Vivo Antiamastigote Activity of *L. Braziliensis*. Intracellular amastigotes were directly extracted from footpad lesions in BALB/c mice previously infected with *L. braziliensis* (MHOM/BZ/82/M2903). The isolate contained amastigotes and small portions of infected macrophages and macrophages. These two last portions were removed from the cellular mixture by controlled centrifugation (at 3000 rpm by 2−3 min) to obtain a culture rich in amastigotes.[32,35,49,50] Amastigote culture was maintained at 37 °C and pH 5.5 in M199 medium (Invitrogen, Leiden, The Netherlands) supplemented with 10% heat-inactivated FCS, 1 g/L L-alanine, 100 mg/L L-asparagine, 200 mg/L sucrose, 50 mg/L sodium pyruvate, 320 mg/L malic acid, 40 mg/L fumaric acid, 70 mg/L succinic acid, 200 mg/L α-ketoglutaric acid, 300 mg/L citric acid, 1.1 g/L sodium bicarbonate, 5 g/L 2-(*N*-morpholino) ethanesulfonic acid (MES), 0.4 mg/L hemin, and 10 mg/L gentamicin. The screening was performed in 96-well microtiter plates maintained at 37 °C. Briefly, 2×10^6 parasites/mL were exposed to increasing concentrations between 1.0 and 50.0 μM (1.0, 5.0, 10.0, 20.0, and 50.0 μM) of each compound **3a**−**f**. Controls contained 1% DMSO. Miltefosine and glucantime were used as reference drugs. The effect of the compound against amastigote forms was tested at 48 h using conventional counting parasites in a Neubauer chamber (optical microscopy, 1000× magnification). Untreated control parasites were used to calculate the relative proliferation.

Cytotoxicity. Peritoneal and J774.1A macrophages were grown in DMEM medium supplemented with 10% heat-inactivated fetal bovine serum, 1% L-glutamine, 1% streptomycin, and 100 units/mL penicillin. Cell viability was assessed using the MTT protocol.[32] Stock solutions (at 25,000 μM) of the tested compounds in DMSO were prepared. Cells were grown in 96-well plates (5×10^4 cells/well) for 24 h. Cultures were carried out at 37 °C in a humidified atmosphere with 5% CO_2 and incubated with the compounds **3a**, **3b**, **3c**, **3d**, **3e**, and **3f** at 10.0, 25.0, 50.0, 75, and 100 μM concentrations for 48 h. After incubation, the medium was removed, and the cells were treated with 100 μL of 0.4 mg/mL MTT for 4 h at 37 °C. Subsequently, 100 μL of DMSO was added to the mixture. The solubilized formazan product was quantified through absorbance measurements at 570 nm. The absorbance values were transformed to the percentage of cytotoxicity compared to the negative controls.

Statistical Analysis. All biological experiments were performed at least three times. The results are expressed as mean ± SD. The Anova test were performed. Only post hoc Dunnet test $p < 0.01$ was considered to be statistically significant. The dose−response curves were plotted using GraphPad prism v.5.02 software.

Mutagenicity Ames Test.[41] *Salmonella typhimurium* TA 98 strain was incubated in agar minimum glucose milieu solution (Difco BactoR agar) and aqueous glucose solution (40%). The direct toxicity of the compound **3c** against *S. typhimurium* TA 98 strain was studied. From these data, the mutagenic assay was performed by incubating **3c** in phosphate buffer (0.1 M, pH 7.4) and DMSO (10% v/v) at six doses, 0.0, 27.9, 37.2, 55.8, 111.7, and 335 μg/plate. The control positive consisted of NPD (20.0 mg/plate), and negative controls consisted of phosphate buffer and DMSO (10% v/v) (0.0 μg/plate of **3c**) solutions. The revertant numbers were counted, and the studied system was considered mutagenic if the colony number was at least double the natural revertants (negative control) for two or more consecutive doses.

Determination of Nitrite Concentration. Nitrite (NO_2^-) accumulation was determined in supernatants of promastigote or epimastigote culture (5×10^6 parasites/well), which were incubated for 5 days in the presence of the active **3c** at increasing concentrations (25, 50, and 100 μM). Three wells with untreated parasites were incubated as the negative control. The assay was performed by the Griess reaction (detection limit: 1.56 μM) with sodium nitrite as a standard as previously described.[34] In brief, 100 μL of Griess reagent 1% sulfanilamide in 50% of acetic acid was added to 400 μL of each sample. The blank reference and standard curve were determined. After 15 min, 100 μL of a solution of *N*-[naphthyl]ethylenediamine dihydrochloride (1%) in acetic acid in 50% was added. The absorbance was measured at 540 nm for that resulting final solution. Nitrite content was quantified by the extrapolation from the sodium nitrite standard curve in each experiment. All the assays were

https://doi.org/10.1021/acsomega.2c06455
ACS Omega 2022, 7, 47225−47238

performed by triplicate. The results were expressed as the amount of nitrite ion (in μM).

Effect of Polyvalent Cations and Folic Acid. These were performed following the protocols of cell viability of promastigote *Leishmania* and epimastigote *T. cruzi*. Details are shown in the Supporting Information.

Theoretical Calculations. All theoretical calculations, in the gas phase, were performed using the B3LYP functional[51] in conjunction with the 6-31G(d,p) basis set[52] using Gaussian09 quantum chemistry software.[53] The geometry of all tested compounds were optimized, and HOMO−LUMO orbital frontiers and EPS were obtained. Theoretical calculations were performed according to the reported strategy for similar structures.[54] HOMO and LUMO frontier orbital maps for compounds and data are shown in Figures S6−S9 and Table S2.

■ ASSOCIATED CONTENT

Supporting Information

The Supporting Information is available free of charge at https://pubs.acs.org/doi/10.1021/acsomega.2c06455.

Full experimental details, emission spectra in the presence of tested acids and their corresponding Stern−Volmer plots, and theoretical data (PDF)

■ AUTHOR INFORMATION

Corresponding Authors

Angel H. Romero − *Grupo de Química Orgánica Medicinal, Instituto de Química Biológica, Facultad de Ciencias, Universidad de la Republica, Montevideo 11400, Uruguay; Laboratorio de Ingeniería Genética, Instituto de Biomedicina, Facultad de Medicina, Universidad Central de Venezuela, Caracas 1073, Venezuela;* orcid.org/0000-0001-8747-5153; Email: angel.ucv.usb@gmail.com

Hugo Cerecetto − *Grupo de Química Orgánica Medicinal, Instituto de Química Biológica, Facultad de Ciencias, Universidad de la Republica, Montevideo 11400, Uruguay; Área de Radiofarmacia, Centro de Investigaciones Nucleares, Facultad de Ciencias, Universidad de la Republica, Montevideo 11400, Uruguay;* orcid.org/0000-0003-1256-3786; Email: hcerecetto@cin.edu.uy

Authors

Elena Aguilera − *Grupo de Química Orgánica Medicinal, Instituto de Química Biológica, Facultad de Ciencias, Universidad de la Republica, Montevideo 11400, Uruguay*

Lourdes Gotopo − *Laboratorio de Síntesis de Orgánica, Facultad de Ciencias, Universidad Central de Venezuela, Caracas 1041-A, Venezuela*

Jaime Charris − *Laboratorio de Síntesis de Medicamentos, Facultad de Farmacia, Universidad Central de Venezuela, Caracas 1041-A, Venezuela*

Noris Rodríguez − *Laboratorio de Ingeniería Genética, Instituto de Biomedicina, Facultad de Medicina, Universidad Central de Venezuela, Caracas 1073, Venezuela*

Henry Oviedo − *Laboratorio de Ingeniería Genética, Instituto de Biomedicina, Facultad de Medicina, Universidad Central de Venezuela, Caracas 1073, Venezuela*

Belén Dávila − *Grupo de Química Orgánica Medicinal, Instituto de Química Biológica, Facultad de Ciencias, Universidad de la Republica, Montevideo 11400, Uruguay*

Gustavo Cabrera − *Laboratorio de Síntesis de Orgánica, Facultad de Ciencias, Universidad Central de Venezuela, Caracas 1041-A, Venezuela*

Complete contact information is available at: https://pubs.acs.org/10.1021/acsomega.2c06455

Author Contributions

A.H.R. performed synthetic experiments and assays for *L. braziliensis* and chemical mechanistic studies, organized the investigation, analyzed the experimental and theoretical data, and prepared and revised the manuscript. E.A. performed biological experiments relative to *L. infantum* and *T. cruzi* and mechanistic biological studies. B.D. performed the Ames Test. L.A.G. performed theoretical experiments. H.O. prepared cultures for in vitro *L. braziliensis* assays. G.C., J.C., N.R., and H.C. provided financial resources. H.C. supervised investigation. H.C. and J.C. revised the manuscript. All authors have given approval to the final version of the manuscript.

Notes

The authors declare no competing financial interest.

■ ACKNOWLEDGMENTS

A.H.R. thanks Agencia Nacional de Investigación e Innovación (ANII) (Uruguay) and CDCH-UCV (Venezuela) for financial support under grant codes PD_NAC_2018_1_150515 and PG-09-8819/2013, respectively. A.H.R., H.C., and E.A. thank further resources from PEDECIBA-QUIMICA (Uruguay) and SNI-ANII (Uruguay). The authors thank Horacio Perazoglo (NMR Laboratory, Universidad de la República) and Dr. Erick Castro (Instituto de Física da UFRGS, Brazil) for NMR spectra and construction of EMM-3D correlations, respectively. Also, the authors are grateful to Copernico Cluster (Universidad Central Venezuela, Caracas, Venezuela) for facilitating calculation.

■ REFERENCES

(1) Kaufer, A.; Ellis, J.; Stark, D.; Barratt, J. The evolution of trypanosomatid taxonomy. *Parasites Vectors* **2017**, *10*, 287.

(2) CDC Global Health. *Infographics-Antibiotic Resistance The Global Threat.*

(3) World Health Organization. Leishmaniasis, https://www.who.int/news-room/fact-sheets/detail/leishmaniasis (accessed in October 2022).

(4) Nwaka, S.; Ridley, R. G. Virtual drug discovery and development for neglected diseases through public-private partnerships. *Nat. Rev. Drug Discovery* **2003**, *2*, 919−928.

(5) (a) Ascenzi, P.; Bocedi, A.; Gradoni, L. The Anti-Parasitic Effects of Nitric Oxide. *IUBMB Life* **2003**, *55*, 573−578. (b) Pavanelli, W. R.; Nogueira Silva, J. J. The Role of Nitric Oxide in Immune Response Against Trypanosoma Cruzi Infection. *Open Nitric Oxide J.* **2010**, *2*, 1−6.

(6) Carneiro, P. P.; Conceição, J.; Macedo, M.; Magalhães, V.; Carvalho, E. M.; Bacellar, O. The Role of Nitric Oxide and Reactive Oxygen Species in the Killing of Leishmania braziliensis by Monocytes from Patients with Cutaneous Leishmaniasis. *PLoS One* **2016**, *11*, No. e0148084.

(7) Almeida-Souza, F.; da Silva, V.; Taniwaki, N. N.; Hardoim, D.; Mendonça Filho, A. R.; Moreira, W. F.; Buarque, C.; Calabrese, K.; Abreu-Silva, A. L. Nitric Oxide Induction in Peritoneal Macrophages by a 1,2,3-Triazole Derivative Improves Its Efficacy upon Leishmania amazonensis In Vitro Infection. *J. Med. Chem.* **2021**, *64*, 12691−12704.

(8) Genestra, M.; Soares-Bezerra, R. J.; Gomes-Silva, L. In vitro sodium nitroprusside-mediated toxicity towards Leishmania amazo-

nensis promastigotes and axenic amastigotes. *Cell Biochem. Funct.* **2008**, *26*, 709−717.
(9) Melo Pereira, J. C.; Carregaro, V.; Costa, D. L.; Santana da Silva, J.; Cunha, F. Q.; Franco, D. W. Antileishmanial activity of ruthenium(II)tetraammine nitrosyl complexes. *Eur. J. Med. Chem.* **2010**, *45*, 4180−4187.
(10) Silva, J. J. N.; Pavanelli, W. R.; Pereira, J. C. M.; Silva, J. S.; Franco, D. W. Experimental Chemotherapy against Trypanosoma cruzi Infection Using Ruthenium Nitric Oxide Donors. *Antimicrob. Agents Chemother.* **2009**, *53*, 4414−4421.
(11) Silva, J. J. N.; Guedes, P. M. M.; Zottis, A.; Balliano, T. L.; Nascimento Silva, F. O.; França Lopes, L. G.; Ellena, J.; Oliva, G.; Andricopulo, A. D.; Franco, D. W.; Silva, J. S. Novel ruthenium complexes as potential drugs for Chagas's disease: enzyme inhibition and in vitro/in vivo trypanocidal activity. *Br. J. Pharmacol.* **2010**, *160*, 260−269.
(12) Fershtat, L. L.; Zhilin, E. S. Recent Advances in the Synthesis and Biomedical Applications of Heterocyclic NO-Donors. *Molecules* **2021**, *26*, 5705.
(13) Boiani, L.; Aguirre, G.; González, M.; Cerecetto, H.; Chidichimo, A.; Cazzulo, J. J.; Bertinaria, M.; Guglielmo, S. Furoxan-, alkylnitrate-derivatives and related compounds as anti-trypanosomatid agents: Mechanism of action studies. *Bioorg. Med. Chem.* **2008**, *16*, 7900−7907.
(14) Hernández, P.; Cabrera, M.; Lavaggi, M. L.; Celano, L.; Tiscornia, I.; Rodrigues da Costa, T.; Thomson, L.; Bollati-Fogolín, M.; Miranda, A. L.; Lima, L. M.; Barreiro, E. J.; González, M.; Cerecetto, H. Discovery of new orally effective analgesic and anti-inflammatory hybrid furoxanyl N-acylhydrazone derivatives. *Bioorg. Med. Chem.* **2012**, *20*, 2158−2171.
(15) Hernández, P.; Rojas, R.; Gilman, R. H.; Sauvain, M.; Lima, L. M.; Barreiro, E. J.; González, M.; Cerecetto, H. Hybrid furoxanyl N-acylhydrazone derivatives as hits for the development of neglected diseases drug candidates. *Eur. J. Med. Chem.* **2013**, *59*, 64−74.
(16) Rehse, K.; Shahrouri, T. Hydrazine Derivatives. *Arch. Pharm.* **1998**, *331*, 308−312.
(17) Jasch, H.; Scheumann, J.; Heinrich, M. R. Regioselective Radical Arylation of Anilines with Arylhydrazines. *J. Org. Chem.* **2012**, *77*, 10699−10706.
(18) Zhang, C.; Jiao, N. Copper-Catalyzed Aerobic Oxidative Dehydrogenative Coupling of Anilines Leading to Aromatic Azo Compounds using Dioxygen as an Oxidant. *Angew. Chem., Int. Ed.* **2010**, *49*, 6174−6177.
(19) Kindt, S.; Jasch, H.; Heinrich, M. R. Manganese(IV)-mediated hydroperoxyarylation of alkenes with aryl hydrazines and dioxygen from air. *Chem.—Eur. J.* **2014**, *20*, 6251−6255.
(20) Kimball, K. F. The mutagenicity of hydrazine and some of its derivatives. *Mutat. Res.* **1977**, *39*, 111−126.
(21) Smith, G. F. Designing Drugs to Avoid Toxicity. *Prog. Med. Chem.* **2011**, *50*, 1−47.
(22) Narang, R.; Narasimhan, B.; Sharma, S. A review on biological activities and chemical synthesis of hydrazide derivatives. *Curr. Med. Chem.* **2012**, *19*, 569−612.
(23) Le Goff, G.; Ouazzani, J. Natural hydrazine-containing compounds: Biosynthesis, isolation, biological activities and synthesis. *Bioorg. Med. Chem.* **2014**, *22*, 6529−6544.
(24) Blair, L. M.; Sperry, J. J. Natural products containing a nitrogen-nitrogen bond. *Nat. Prod.* **2013**, *76*, 794−812.
(25) Burke, A. A.; Severson, E. S.; Mool, S.; Solares Bucaro, M. J.; Greenaway, F. T.; Jakobsche, C. E. Comparing hydrazine-derived reactive groups as inhibitors of quinone-dependent amine oxidases. *J. Enzyme Inhib. Med. Chem.* **2017**, *32*, 496−503.
(26) Hampannavar, G. A.; Karpoormath, R.; Palkar, M. B.; Shaikh, M. S.; Chandrasekaran, B. Dehydrozingerone Inspired Styryl Hydrazine Thiazole Hybrids as Promising Class of Antimycobacterial Agents. *ACS Med. Chem. Lett.* **2016**, *7*, 686−691.
(27) Ahn, J. H.; Shin, M. S.; Jun, M. A.; Jung, S. H.; Kang, S. K.; Kim, KR.; Rhee, S. D.; Kang, N. S.; Kim, S. Y.; Sohn, S. K.; Kim, S. G.; Jin, M. S.; Lee, J. O.; Cheon, H. G.; Kim, S. S. Synthesis, biological evaluation and structural determination of β-aminoacyl-containing cyclic hydrazine derivatives as dipeptidyl peptidase IV (DPP-IV) inhibitors. *Bioorg. Med. Chem. Lett.* **2007**, *17*, 2622−2628.
(28) Dascalu, A. E.; Ghinet, A.; Lipka, E.; Furman, C.; Rigo, B.; Fayeulle, A.; Billamboz, M. Design, synthesis and evaluation of hydrazine and acyl hydrazone derivatives of 5-pyrrolidin-2-one as antifungal agents. *Bioorg. Med. Chem. Lett.* **2020**, *30*, 127220.
(29) Dehghani, Z.; Khoshneviszadeh, M.; Khoshneviszadeh, M.; Ranjbar, S. Veratric acid derivatives containing benzylidene-hydrazine moieties as promising tyrosinase inhibitors and free radical scavengers. *Bioorg. Med. Chem.* **2019**, *27*, 2644−2651.
(30) Quiliano, M.; Pabón, A.; Ramirez-Calderon, G.; Barea, C.; Deharo, E.; Galiano, S.; Aldana, I. New hydrazine and hydrazide quinoxaline 1,4-di-N-oxide derivatives: In silico ADMET, antiplasmodial and antileishmanial activity. *Bioorg. Med. Chem. Lett.* **2017**, *27*, 1820−1825.
(31) Soares, R. R.; Antinarelli, L. L.; Souza, V. F.; Souza, F.; Lopes, K. G.; Scopel, S.; Coimbra, D.; Silva, C.; Abramo, C. In Vivo Antimalarial and In Vitro Antileishmanial Activity of 4- Aminoquinoline Derivatives Hybridized to Isoniazid or Sulfa or Hydrazine Groups. *Lett. Drug Des. Discovery* **2017**, *14*, 597−604.
(32) Romero, A. H.; Rodríguez, N.; Oviedo, H. 2-Aryl-quinazolin-4(3H)-ones as an inhibitor of leishmania folate pathway: In vitro biological evaluation, mechanism studies and molecular docking. *Bioorg. Chem.* **2019**, *83*, 145−153.
(33) López, S.; Salazar, J.; López, S. E. A Simple One-Pot Synthesis of 2-Substituted Quinazolin-4(3H)-ones from 2-Nitrobenzamides by Using Sodium Dithionite. *Synthesis* **2013**, *45*, 2043−2050.
(34) Romero, A. H.; Medina, R.; Alcala, A. M.; García-Marchan, Y.; Núñez-Duran, J.; Leañez, J.; Mijoba, A.; Ciangherotti, C.; Serrano-Martín, X.; López, S. E. Design, synthesis, structure-activity relationship and mechanism of action studies of a series of 4-chloro-1-phthalazinyl hydrazones as a potent agent against Leishmania braziliensis. *Eur. J. Med. Chem.* **2017**, *127*, 606−620.
(35) Romero, A. H.; Rodríguez, N.; Oviedo, S. E.; Lopez, H. Antileismanial activity, mechanism of action study and molecular docking of 1,4-bis(substituted benzalhydrazino)phthalazines. *Arch. Pharm.* **2019**, *352*, No. e1800299.
(36) Álvarez, G.; Martínez, J.; Varela, J.; Birriel, E.; Cruces, E.; Gabay, M.; Leal, S. M.; Escobar, P.; Aguirre-López, B.; Cabrera, N.; Tuena-de Gómez-Puyou, M.; Gómez-Puyou, A.; Pérez-Montfort, R.; Yaluff, G.; Torres, S.; Serna, E.; Vera de Bilbao, N.; González, M.; Cerecetto, H. Development of bis-thiazoles as inhibitors of triosephosphate isomerase from Trypanosoma cruzi. Identification of new non-mutagenic agents that are active in vivo. *Eur. J. Med. Chem.* **2015**, *100*, 246−256.
(37) Swiss-ADME, Swiss Institute of Bioinformatics. http://www.swissadme.ch/index.php (accessed in August 2022).
(38) Lipinski, C. A.; Lombardo, F.; Dominy, B. W.; Feeney, P. J. Experimental and computational approaches to estimate solubility and permeability in drug discovery and development settings. *Adv. Drug Deliv. Rev.* **2001**, *46*, 3−26.
(39) Daina, A.; Michielin, O.; Zoete, V. SwissADME: a free web tool to evaluate pharmacokinetics, drug-likeness and medicinal chemistry friendliness of small molecules. *Sci. Rep.* **2017**, *7*, 42717.
(40) Baell, J. B.; Holloway, G. A. New Substructure Filters for Removal of Pan Assay Interference Compounds (PAINS) from Screening Libraries and for Their Exclusion in Bioassays. *J. Med. Chem.* **2010**, *53*, 2719−2740.
(41) Cariello, N. F.; Piegorsch, W. W. The Ames test: The two-fold rule revisited. *Mutat. Res.* **1996**, *369*, 23−31.
(42) Gilbert, I. H. Inhibitors of dihydrofolate reductase in Leishmania and trypanosomes. *Biochem. Biophys. Acta* **2002**, *1587*, 249−257.
(43) Kumar, A. S.; Kudva, J.; Lahtinen, M.; Peuronen, A.; Sadashiva, R.; Naral, D. Synthesis, characterization, crystal structures and biological screening of 4-amino quinazoline sulfonamide derivatives. *J. Mol. Struct.* **2019**, *1190*, 29−36.

https://doi.org/10.1021/acsomega.2c06455
ACS Omega 2022, 7, 47225−47238

(44) Suzuki, Y.; Sawada, J.; Hibner, M.; Ishii, A.; Matsuno, R.; Sato, D.; Witulski, B.; Asai, A. Fluorescent anticancer quinazolines as molecular probes for β-tubulin colchicine site competition assay and visualization of microtubules as intracellular targeting sites. *Dyes Pigments* **2017**, *145*, 233−238.
(45) Motoyama, M.; Doan, J.; Hibner-Kulicka, M.; Otake, A.; Lukarska, R.; Lohier, D. Synthesis and Structure-Photophysics Evaluation of 2-N-Amino-quinazolines: Small Molecule Fluorophores for Solution and Solid State. *Chem.—Asian J.* **2021**, *16*, 2087−2099.
(46) Held, F. E.; Guryev, J.; Fröhlich, M.; Hampel, A.; Kahnt, R.; Hutterer, D. Facile access to potent antiviral quinazoline heterocycles with fluorescence properties via merging metal-free domino reactions. *Nat. Commun.* **2017**, *8*, 15071.
(47) Romero, A. H.; Romero, I. E.; Piro, O. E.; Echeverría, G. A.; Gotopo, L.; Moller, M. N.; Rodríguez, G. A.; Cabrera, G. J.; Castro, E. R.; López, S. E.; Cerecetto, H. Photo-Induced Partially Aromatized Intramolecular Charge Transfer. *J. Phys. Chem. B* **2021**, *125*, 9268−9285.
(48) Miranda, K. M. The chemistry of nitroxyl (HNO) and implications in biology. *Coord. Chem. Rev.* **2005**, *249*, 433−455.
(49) Romero, A. H.; Rodríguez, N.; López, S. E.; Oviedo, H. Identification of dehydroxy isoquine and isotebuquine as promising antileishmanial agents. *Arch. Pharm.* **2019**, *352*, 1800281.
(50) Romero, A. H.; Rodríguez, N.; Ramírez, O. G. Optimization of phthalazin-based aryl/heteroarylhydrazones to design new promising antileishmanicidal agents: Synthesis and biological evaluation of 3-aryl-6-piperazin-1,2,4-triazolo[3,4-a]phthalazines. *New J. Chem.* **2020**, *44*, 13807−13814.
(51) Becke, A. D. A new mixing of Hartree−Fock and local density-functional theories. *J. Chem. Phys.* **1993**, *98*, 1372.
(52) Petersson, G. A.; Al-Laham, M. A. A complete basis set model chemistry. II. Open-shell systems and the total energies of the first-row atoms. *J. Chem. Phys.* **1991**, *94*, 6081.
(53) Frisch, M. J.; Trucks, G. W.; Schlegel, H. B.; Scuseria, G. E.; Robb, M. A.; Cheeseman, J. R.; Scalmani, G.; Barone, V.; Mennucci, B.; Petersson, G. A.; et al. *Gaussian 09*, Revision A.1; Gaussian, Inc.: Wallingford, CT, 2009.
(54) Acosta, M.; Gotopo, L.; Gamboa, N.; Rodrigues, J.; Henriques, G.; Cabrera, G.; Romero, A. H. Antimalarial Activity of Highly Coordinative Fused-Heterocycles Targeting β-Hematin Crystallization. *ACS Omega* **2022**, *7*, 7499−7514.

https://doi.org/10.1021/acsomega.2c06455
ACS Omega 2022, 7, 47225−47238